

Amphiphilic hard body mixtures

Matthias Schmidt and Christian von Ferber

Institut für Theoretische Physik II, Heinrich-Heine-Universität Düsseldorf, Universitätsstraße 1, D-40225 Düsseldorf, Germany

(Received 16 June 2001; published 29 October 2001)

In order to study ternary amphiphilic mixtures, we introduce a simplistic model of hard spheres corresponding to water and hard needles corresponding to oil and amphiphilic particles, where the hydrophilic head is modeled as a hard sphere and the hydrophobic tail as an infinitely thin needle attached radially to the sphere. For this system, we construct a geometry-based density functional and perform Monte Carlo computer simulations. The equation of state derived from the theory is found to be in remarkable agreement with our simulation results. We investigate the theoretical demixing phase diagram, and find that the predicted trends strongly support the amphiphilic character of the model.

DOI: 10.1103/PhysRevE.64.051115

PACS number(s): 82.70.Uv, 61.20.Gy, 64.70.Ja

I. INTRODUCTION

Adding amphiphiles to a system of oil and water considerably enhances the miscibility of these substances. Amphiphilic molecules consist of a hydrophilic head group and a hydrophobic tail, which prefer being dissolved in water and oil, respectively. The physics of amphiphilic systems is important in many areas, including industrial and domestic applications like washing, cleaning, emulsification, and many more. Due to the different preferences of their constituents, amphiphiles adsorb at oil-water interfaces and facilitate the creation of such interfaces. Depending on the thermodynamical variables, these interfaces arrange in a rich variety of structures [1–4], and much theoretical work has been devoted to understanding the underlying basic mechanisms. Microscopic approaches have often used a lattice fluid model [5–8], while coarse grained continuum descriptions are provided by Ginzburg-Landau [9] or integral geometrical [10] models.

Density functional theory (DFT) [11] is a powerful approach to inhomogeneous statistical systems, and has been applied to study amphiphilic behavior on different levels from microscopic to macroscopic. A model for membranes, vesicles, and micelles [12] based on a description for effective amphiphile interactions arising from the presence of solvent molecules has been studied. The phase behavior of a symmetrical ternary mixture was found to exhibit three-(isotropic)-liquid-phase coexistence [13]. This approach was generalized to asymmetric interactions between amphiphiles and water and oil, and lamellar and micellar phases were found [14]. The structure of droplet microemulsions was also treated [15]. The problem of separation of length scales into those of the microscopic domain (relevant for building up interfaces) and those of the mesoscopic regime (to capture the degrees of freedom of supramolecular aggregates) was addressed within a one-dimensional model of molecular aggregation [16], and later on generalized to the three-dimensional case [17]. The phase behavior [18] and gas-liquid nucleation [19] of amphiphilic binary mixtures consisting of Lennard-Jones monomers and bonded dimers has been investigated. Furthermore, a DFT approach has been applied to nucleation in micellar solutions [20].

In this work we propose a simple atomistic model in order

to investigate amphiphilic mixtures. The particles possess continuous (off-lattice) positions and orientations, and we prescribe the microscopic interparticle interactions. In our model, only hard core pair interactions are present; hence the behavior is solely driven by entropy. Using hard core systems has proved to be fruitful for important phenomena like freezing [21] and liquid crystalline ordering, and we believe that this could also be the case for amphiphiles. To study the model, we construct a geometry-based DFT. This approach originates from Rosenfeld's fundamental measure theory for hard sphere mixtures [22–25], which was also formulated for convex bodies [26] and parallel hard cubes [27,28]. Recently, within geometry-based DFT, a range of models has been treated successfully, including the Asakura-Oosawa colloid-ideal-polymer mixture [29], the Widom-Rowlinson model [30], and a model due to Bolhuis and Frenkel [31], where hard spheres are mixed with infinitely thin needles [32]. This needle-sphere mixture displays a demixing phase transition crudely reminiscent of that of water and oil. Here, we use this as a starting point, and supplement it with a third species of particle that consists of a sphere to which a needle is attached rigidly. The spherical part is a caricature of the hydrophilic head and the needle models the hydrophobic tail of an amphiphilic molecule. Hence we arrive at a simplistic model for a nonionic amphiphile ternary mixture, featuring explicit water-oil asymmetry. Hybrid shapes of spheres and (thin) rods are also realized in the colloidal domain by microtubules inside vesicles [33,34], and by rodlike fd bacteriophage viruses bound to silica beads [35].

As will be seen below, our hard body amphiphiles are nonconvex particles. In order to deal with nonconvexity, we carry over the recipes developed for convex particles [32], at the expense of a certain violation of the overlap condition within the theory. As we will show in detail, the violation is quantitatively small and does not hinder the development of a powerful theory.

Our final aim is to elucidate the phase behavior of the system. To have benchmark results to test the theory against, we have carried out Monte Carlo (MC) computer simulations, and have obtained results for the equation of state for typical compositions of species and over a broad range of densities in regions where the system remains in a fluid state. Comparing with the theoretical results, we find nice agree-

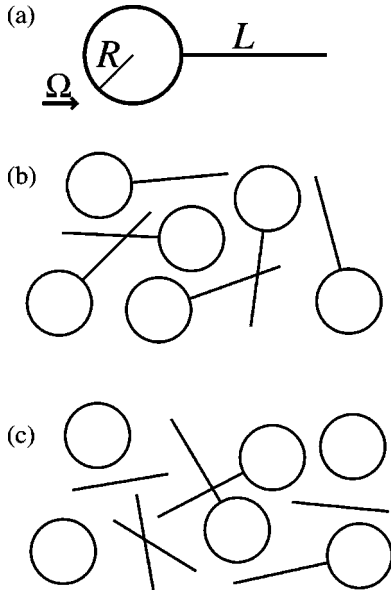


FIG. 1. Sketch of the model amphiphilic mixture. (a) Amphiphilic molecules consisting of a hard, infinitely thin needle of length L , which is attached radially to a hard sphere of radius R . The orientation of the particle is described by the unit vector Ω . (b) Pure amphiphile system. (c) Ternary system consisting of amphiphiles, hard spheres (water), and hard, infinitely thin needles (oil).

ment, and hence are confident in trusting the theoretical results for the phase diagram, without further checking against simulations. We find that amphiphiles mix better with either spheres or needles than do spheres with needles. The ratio of tail length to head radius acts as a control parameter governing the relative affinity of amphiphiles for either spheres or needles.

The paper is organized as follows. In Sec. II we define the ternary hard body mixture of amphiphiles, spheres, and needles, as well as a multicomponent generalization thereof. In Sec. III we develop the DFT first for this general system, and then specialize to the actual ternary mixture as well as to a pure system of amphiphiles. We also discuss the problem arising from the nonconvexity of the particles. Our computer simulation technique is presented in Sec. IV. In Sec. V we investigate demixing phase behavior for homogeneous fluid states. Discussion and an outlook are given in the concluding Sec. VI.

II. THE MODEL

Let us introduce amphiphilic hard core particles, which consist of a hard sphere of radius R and an infinitely thin needle of length L . The needle (tail) is attached radially to the sphere (head); see Fig. 1(a) for a sketch of the resulting geometrical shape. The direction of the needle is denoted by Ω . A single-component system of amphiphiles [see Fig. 1(b) for an illustration] is ruled by the number density ρ_A . We refer to this system in the following as *pure amphiphiles*; see Fig. 2(a) for a snapshot from a computer simulation (de-

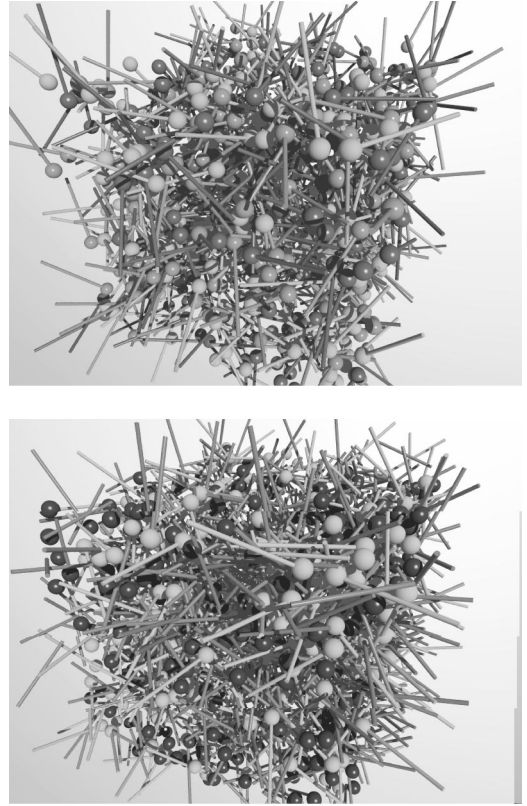


FIG. 2. Snapshots from computer simulation. (a) Pure amphiphile system; the particles possess different gray levels. (b) Ternary mixture of spheres (black), needles (gray), and amphiphiles (white).

scribed below) of this model.

We also consider a three-component mixture of (i) particles with amphiphilic character, (ii) particles corresponding to water, and (iii) particles corresponding to oil molecules. For our amphiphiles (species A), adding two further species for which their shape possesses an amphiphilic character is straightforward. We use hard spheres (species S) with radius R as a caricature of water. The role of oil is played by hard, infinitely thin needles (species N) of length L . Hence we arrive at a model that we refer to as the *ternary mixture*; see Fig. 1(c) for a sketch. The number densities are denoted by $\rho_i, i=A, N, S$, the sphere diameter by $\sigma=2R$, and the size ratio by $q=L/R$. The packing fraction of spheres is $\eta_S = 4\pi R^3 \rho_S/3$, and that of amphiphilic heads is $\eta_A = 4\pi R^3 \rho_A/3$. We show a typical particle configuration in Fig. 2(b) as an illustration.

Additionally, we generalize to a multicomponent mixture where the species are labeled by i (adopting a discrete picture of mixtures); the spherical head groups of species i possess radii R_i and the needle tails have lengths L_i . This *multicomponent mixture* will be used below to formulate the DFT. Clearly, it includes the case of monodisperse amphiphiles, if only a single species A is present. Also the ternary mixture is obtained as a special case. For $i=A, N, S$, we simply set $L_A = L_N$, $L_S=0$, $R_A=R_S$, and $R_N=0$.

III. THEORY

A. Density functional

The DFT we propose is a weighted density approximation. By convolutions of the position- and orientation-dependent density profiles $\rho_i(\mathbf{r}, \mathbf{\Omega})$, weighted densities are obtained. These weighted densities are converted by a simple function into an excess free energy density. This is a local quantity, depending on space point and orientation. The global excess free energy is obtained by integration over space and rotator degree of freedom. The weight functions with which the $\rho_i(\mathbf{r}, \mathbf{\Omega})$ are convoluted are obtained by geometric considerations and describe the geometrical shapes of the particles. We first formulate the theory for the general multicomponent mixture, and then specialize to pure amphiphiles as well as to the ternary mixture.

1. Multicomponent amphiphiles

We start by giving the weight functions. Those that are characteristic functions of the needle part of the particles are defined as

$$\bar{w}_q^{(i)}(\mathbf{r}, \mathbf{\Omega}) = \frac{1}{4} \int_{R_4}^{R_i+L_i} dl \delta(\mathbf{r}+l\mathbf{\Omega}), \quad (1)$$

$$\bar{w}_0^{(i)}(\mathbf{r}, \mathbf{\Omega}) = \frac{1}{2} [\delta(\mathbf{r}+(R_i+L_i)\mathbf{\Omega}) - \delta(\mathbf{r}+R_i\mathbf{\Omega})]. \quad (2)$$

Here and in the following, the overbar indicates needle (tail) quantities. The weight functions that describe the sphere part of the particles are equal to those for pure hard spheres (HS's) [22,25] and are defined as

$$w_3^{(i)}(\mathbf{r}) = \theta(R_i-r), \quad w_2^{(i)}(\mathbf{r}) = \delta(R_i-r), \quad (3)$$

$$\mathbf{w}_{v2}^{(i)}(\mathbf{r}) = w_2^{(i)}(\mathbf{r}) \cdot \mathbf{r}/r, \quad \hat{\mathbf{w}}_{m2}^{(i)}(\mathbf{r}) = w_2^{(i)}(\mathbf{r}) [\mathbf{r}\mathbf{r}/r^2 - \hat{\mathbf{1}}/3], \quad (4)$$

$$\bar{w}_2^{(i)}(\mathbf{r}, \mathbf{\Omega}) = 2|\mathbf{w}_{v2}^{(i)}(\mathbf{r}) \cdot \mathbf{\Omega}|, \quad (5)$$

where $r=|\mathbf{r}|$, $\theta(r)$ is the step function, and $\hat{\mathbf{1}}$ is the identity matrix. Further, linearly dependent, weights are $w_1^{(i)}(\mathbf{r}) = w_2^{(i)}(\mathbf{r})/(4\pi R_i)$, $\mathbf{w}_{v1}^{(i)}(\mathbf{r}) = \mathbf{w}_{v2}^{(i)}(\mathbf{r})/(4\pi R_i)$, and $w_0^{(i)}(\mathbf{r}) = w_1^{(i)}(\mathbf{r})/R_i$. The weight functions possess different tensorial rank: $w_0^{(i)}$, $w_1^{(i)}$, $w_2^{(i)}$, and $w_3^{(i)}$ are scalars; $\mathbf{w}_{v1}^{(i)}$ and $\mathbf{w}_{v2}^{(i)}$ are vectors; $\hat{\mathbf{w}}_{m2}^{(i)}$ is a (traceless) matrix. The weighted densities are

$$n_\nu(\mathbf{r}) = \sum_i \int \frac{d^2\Omega'}{4\pi} \rho_i(\mathbf{r}', \mathbf{\Omega}') * w_\nu^{(i)}(\mathbf{r}''), \quad (6)$$

$$\bar{n}_\nu(\mathbf{r}, \mathbf{\Omega}) = \sum_i \rho_i(\mathbf{r}', \mathbf{\Omega}') * \bar{w}_\nu^{(i)}(\mathbf{r}'', \mathbf{\Omega}''), \quad \nu=0,1, \quad (7)$$

$$\bar{n}_2(\mathbf{r}, \mathbf{\Omega}) = \sum_i \int \frac{d^2\Omega'}{4\pi} \rho_i(\mathbf{r}', \mathbf{\Omega}') * \bar{w}_2^{(i)}(\mathbf{r}'', \mathbf{\Omega}''), \quad (8)$$

where the star denotes convolution, $g(\mathbf{r}') * h(\mathbf{r}'') = \int d^3x g(\mathbf{x}) h(\mathbf{r}-\mathbf{x})$. The Helmholtz free energy is $F = F^{\text{id}} + F^{\text{exc}}$, where F^{exc} arises from interactions and the ideal gas contribution is

$$F^{\text{id}}[\rho_i(\mathbf{r}, \mathbf{\Omega})] = \sum_i \int d^3x \int \frac{d^2\Omega}{4\pi} \rho_i(\mathbf{r}, \mathbf{\Omega}) \times \{\ln[\rho_i(\mathbf{r}, \mathbf{\Omega}) \Lambda_i^3] - 1\}, \quad (9)$$

where Λ_i is the thermal wavelength of species i . [Note that the normalization is such that $\rho(\mathbf{r}, \mathbf{\Omega}) = \rho(\mathbf{r})$ for isotropic orientation distributions.] The excess free energy is

$$F^{\text{exc}}[\{\rho_i(\mathbf{r}, \mathbf{\Omega})\}] = k_B T \int d^3r \int \frac{d^2\Omega}{4\pi} \Phi(\{n_\gamma\}, \{\bar{n}_\gamma\}), \quad (10)$$

where k_B is Boltzmann's constant and T the temperature, and the (local) free energy density Φ is a simple function (not a functional) of the weighted densities n_γ . Considering multicavity distributions [25], we obtain $\Phi = \Phi_{\text{HS}} + \bar{\Phi}$ with

$$\begin{aligned} \Phi_{\text{HS}} = & -n_0 \ln(1-n_3) + (n_1 n_2 - \mathbf{n}_{v1} \cdot \mathbf{n}_{v2}) / (1-n_3) \\ & + [(n_2)^3/3 - n_2(\mathbf{n}_{v2})^2 + 3(\mathbf{n}_{v2} \cdot \hat{\mathbf{n}}_{m2} \cdot \mathbf{n}_{v2} \\ & - 3 \det \hat{\mathbf{n}}_{m2})/2] / [8\pi(1-n_3)^2], \end{aligned} \quad (11)$$

which is equal to the pure HS case [22,25]. The contribution due to the presence of the needles is

$$\Phi = -\bar{n}_0 \ln(1-n_3) + \frac{\bar{n}_1 \bar{n}_2}{1-n_3}. \quad (12)$$

This completes the prescription for the functional for multicomponent amphiphiles.

2. Pure amphiphiles

For a one-component system of amphiphile particles with radius R and needle length L , the general functional can easily be reduced. The summations over species i in Eqs. (6)–(8) vanish, and a density functional of a single density field $\rho_A(\mathbf{r}, \mathbf{\Omega})$ is obtained.

3. Ternary mixture

We consider a mixture of spheres (species S) with radii R , needles (species N) with length L , and amphiphiles (species A) with the same dimensions, namely, radius R and length L . The weight functions for spheres ($L_S=0$) simplify, such that $\bar{w}_0^{(S)} = \bar{w}_1^{(S)} = 0$, and $\bar{w}_2^{(S)}$ is identical to the corresponding weight function in the case of the needle-sphere functional [32]. All $w_\nu^{(S)}$ are identical to those of the pure hard sphere case [22,25]. For needles, all densities with $\nu > 1$ vanish, $w_\nu^{(N)} = 0$. This is expected from dimensional arguments, because an infinitely thin needle does not possess surface area ($\nu=2$), nor volume ($\nu=3$). The remaining weight function $w_1^{(N)}$ is identical to that in the case of the needle-sphere functional. The weight function for $\nu=0$ is also identical to that

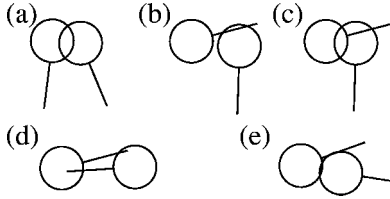


FIG. 3. Configurations of overlapping amphiphiles. Cases where the Mayer function is correct within the DFT, $f = -1$: (a) sphere-sphere; (b) sphere-needle; (c) sphere overlapping simultaneously with the needle and the sphere of a second particle. Problem cases, where $f = -2$ within the DFT: (d) simultaneous sphere-needle overlap; (e) sphere overlapping with the needle and the sphere of the second particle, so that the inner needle end point is outside the first sphere.

in this case, and is obtained as the sum $w_0^{(N)} + \bar{w}_0^{(N)}$. Note that in the present description the position coordinate of the needle is one of its end points, whereas using the needle midpoint might be more intuitive (see Ref. [32]). Both descriptions are of course equivalent, and are related by a simple coordinate transformation.

B. Mayer bonds

The Mayer f_{ij} bond between species i and j is $f_{ij} = -1$, if the two particles overlap, and zero otherwise. Within geometry-based DFT, the f_{ij} are represented as the (negative) Euler characteristics of the overlap region of the two bodies i and j . For convex bodies, the overlap region is also convex, and hence carries Euler characteristic of unity. For nonconvex bodies the situation is more complicated. The overlap region may consist of several disconnected portions, and its Euler characteristic equals the number of these portions.

For our model, the two-particle Mayer bonds are correct within the DFT, if no amphiphile is involved, i.e., f_{SS} and f_{SN} . Furthermore, f_{AN} is also correct. Problems arise between two amphiphiles, f_{AA} , as well as between an amphiphile and a sphere, f_{AS} . In Figs. 3(a-c) we display the cases where the Mayer bond is correct, and Figs. 3(d,e) show the cases where the Mayer bond is incorrect, namely, $f_{ij} = -2$. It might be physically expected that the statistical weight of such problem configurations is only small, because for a given position and orientation of the first particle the second particle's position *and* orientation are restricted.

C. Second virial coefficients

In order to measure quantitatively the degree of violation of the overlap condition, we evaluate the second virial coefficient for amphiphiles from the DFT and compare it to the exact result, which we can obtain analytically. Note that this is precisely a test of the accuracy of the present approach in the low-density limit. For simplicity, we perform the calculation for pure amphiphiles. The second virial coefficient is defined as

$$B_{2,ij} = -\frac{1}{2V} \int d^3r d^2\Omega d^3r' d^2\Omega' f_{ij}(\mathbf{r}, \mathbf{\Omega}; \mathbf{r}', \mathbf{\Omega}'), \quad (13)$$

TABLE I. Overview of simulated systems. Particle numbers (#) for needles (N), amphiphiles (A), and spheres (S) are given. η_{tot} denotes the total packing fraction of *spherical* entities.

| | Species | # N | # A | # S | η_{tot} |
|---------|---------|-------|-------|-------|---------------------|
| Pure | A | | 1000 | | η_A |
| | S | | | 1000 | η_S |
| Binary | AN | 1000 | 1000 | | η_A |
| | SN | 1000 | | 1000 | η_S |
| | AS | | 500 | 500 | $\eta_A + \eta_S$ |
| Ternary | ASN | 1000 | 500 | 500 | $\eta_A + \eta_S$ |
| | | 1000 | 500 | 1000 | |
| | | 1000 | 1000 | 500 | |

where V is the system volume. We find the exact result for pure amphiphiles as

$$B_{2,AA}^{\text{exact}} = \frac{16\pi^3}{15(L+R)^2} \left\{ -2L^5 - 10L^4R + 5L^3R^2 + 5(25 + 6\sqrt{3}) \times L^2R^3 + 5(41 + 12\sqrt{3})LR^4 + (91 + 30\sqrt{3})R^5 + 2[R^2 + (L+R)^2]^{5/2} \right\}, \quad (14)$$

which holds for the case $L > (\sqrt{3} - 1)R$. For $L \gg R$, the expansion is

$$B_{2,AA}^{\text{exact}} = 16\pi^3 \left[2LR^2 + \left(\frac{20}{3} + 2\sqrt{3} \right) R^3 + O\left(\frac{R^4}{L} \right) \right], \quad (15)$$

where $20/3 + 2\sqrt{3} = 10.1308$. The result from DFT is

$$B_{2,AA}^{\text{DFT}} = 16\pi^3 \left(2LR^2 + \frac{32}{3} R^3 \right), \quad (16)$$

which is free of terms of order R^4/L and higher. Note that the term of order LR^2 is the dominant contribution from sphere-needle overlap. This is exact in the DFT. The term of order R^3 stems from the hard core between spheres, and is overestimated by about 5% in the DFT. All higher-order corrections are not reproduced in the DFT result. We conclude that for $L \gg R$ the DFT result is an excellent approximation to $B_{2,AA}^{\text{exact}}$. Even for $L/R = 10$, the relative deviation is only $B_{2,AA}^{\text{DFT}}/B_{2,AA}^{\text{exact}} = 1.017$. For shorter needles, $L = R$, the deviation grows somewhat to $B_{2,AA}^{\text{DFT}}/B_{2,AA}^{\text{exact}} = 1.036$.

IV. COMPUTER SIMULATION

We use the canonical ensemble to carry out Monte Carlo simulations. Our method of obtaining the pressure is based on the probability density of a successful small change in system volume. In order to perform such a compression, we enlarge the dimensions of each particle by a factor $1 + \alpha$, where $\alpha = 0.00125 - 0.005$, and test for overlap. The statistics of this test yields the pressure p .

We have carried out simulations at 48 state points with different densities and compositions of species. At each state point 10^4 Monte Carlo cycles were done. Particle numbers range from 1000 to 2500 particles; see Table I for details. As

a compromise between considerable needle length and manageable simulation box size, we pick the size ratio $q=L/R=10$ for all runs. The simulation box is chosen to be larger than twice the particle length in order to avoid problems with multiple overlap of periodic images. In terms of the total packing fraction $\eta_{\text{tot}}=\eta_A+\eta_S$, we simulate in the range $\eta=0.05-0.3$ by varying the simulation box size.

V. FLUID PHASES

We proceed from simple to complex, and hence start with a discussion of one-component fluid phases, in particular, of the pure amphiphile system. We then turn to the (three) binary systems that are obtained by selecting pairs out of the three species. Formally, these are obtained from the ternary sphere-amphiphile-needle system by setting the density of one of the species to zero. Finally, we investigate the full ternary mixture.

In the following we restrict ourselves to homogeneous, isotropic fluid states, which are characterized by spatially and rotationally invariant density distributions, $\rho_i(\mathbf{r},\mathbf{\Omega})=\text{const}$. Any mesophases, like lamellar or micellar ones, as well as liquid crystalline ordering, are explicitly excluded from our investigation. However, such density distributions allow for phase separation into macroscopically demixed phases. The strategy is to apply the DFT to the homogeneous densities and hence to derive the bulk free energy and the equation of state. This task can be performed analytically within the present theory. We then check the numerical accuracy of the equation of state obtained via differentiation of the free energy against computer simulation results. Finally, we calculate the theoretical demixing phase diagrams including binodal, spinodal, and critical point for the binary mixtures. In the final case of the ternary mixture, we restrict ourselves to the spinodal.

In detail, our calculations are as follows. For homogeneous, isotropic states, the weighted densities become proportional to the bulk density $n_\nu=\sum_i \xi_\nu^{(i)} \rho_i$. The proportionality constants are given as fundamental measures $\xi_\nu^{(i)}=\int d^3r w_\nu^{(i)}(\mathbf{r})$. For the ternary case, the fundamental measures are for spheres $\xi_3^S=4\pi R^3$, $\xi_2^S=4\pi R^2$, $\xi_1^S=R$, $\xi_0^S=1$, for amphiphiles $\xi_3^A=4\pi R^3$, $\xi_2^A=4\pi R^2$, $\xi_1^A=R+L/4$, $\xi_0^A=1$, and for needles $\xi_1^N=L/4$, $\xi_0^N=1$. Note that, although an amphiphile consist of a sphere and a needle, $\xi_\nu^A=\xi_\nu^S+\xi_\nu^N$ does not hold for all ν . This is because $\xi_0^{(i)}=1$ for all species, because each particle consists of a single body and hence possesses Euler characteristic unity. Hence the weighted densities in isotropic bulk fluids become $n_3=4\pi R^3(\rho_S+\rho_A)/3(=\eta_{\text{tot}})$, $n_2=4\pi R^2(\rho_S+\rho_A)(=3\eta_{\text{tot}}/R)$, $n_1=R(\rho_S+\rho_A)[=3\eta_{\text{tot}}/(4\pi R^2)]$, $n_0=\rho_S+\rho_A[=3\eta_{\text{tot}}/(4\pi R^3)]$, and $\bar{n}_1=(\rho_N+\rho_A)L/4$, $\bar{n}_0=\rho_N$.

We obtain the spinodal for demixing from the bulk free energy by solution of $\det \partial^2(F/V)/\partial \rho_i \partial \rho_j=0$, which indicates the boundary of stability. This was carried out previously for the case of the binary needle-sphere mixture ($\rho_A=0$) [32], and a *universal* (q -independent) spinodal was found. Here we follow the same recipe for the remaining two binary mixtures, namely, (i) adding needles to pure amphiphiles and (ii)

adding spheres to pure amphiphiles. For the full ternary mixture, we can also, somewhat surprisingly, find an analytical expression for the spinodal depending on all three densities.

In the case of one-component hard spheres our theory reduces to the Rosenfeld functional [22] in Tarazona's latest tensorial version [25]. The excess free energy density per volume for pure hard spheres with packing fraction η and radius R derived from the DFT is identical to the result of the Percus-Yevick compressibility (scaled-particle) approximation, and is given as $\beta F^{\text{exc}}(\eta_S)/V=\Phi_{\text{HS}}$, where $\beta=1/k_B T$ and

$$\Phi_{\text{HS}}(\eta)=\frac{3\eta[3\eta(2-\eta)-2(1-\eta)^2\ln(1-\eta)]}{8\pi R^3(1-\eta)^2}. \quad (17)$$

The pure system of needles constitutes an ideal gas of (non-interacting) rotators. Hence the excess free energy vanishes exactly, and indeed we recover this (trivial) result, $\Phi=0$. This is merely a check of the above method (Sec III A) for generating DFTs from the zero-dimensional limit, and demonstrates that this does not lead to artificial interactions.

A. Pure amphiphiles

The system of one-component amphiphiles provides a first nontrivial test case. For the homogeneous, isotropic bulk phase $\rho_A(\mathbf{r},\mathbf{\Omega})=\text{const}$, we obtain the excess Helmholtz free energy per volume $\beta F^{\text{exc}}/V=\Phi_A$, with

$$\Phi_A=\Phi_{\text{HS}}(\eta_A)+\frac{9q\eta_A^2}{16\pi R^3(1-\eta_A)}. \quad (18)$$

In this additive expression, Φ_{HS} is the residual contribution for $q=0$, stemming only from the presence of the spherical heads. The contribution due to the presence of the needle tails scales *linearly* with size ratio q . The dependence on η_A is a rational expression typical of geometry-based DFT, with a (formal) divergence $\eta_A\rightarrow 1$. Clearly, for large q this second term dominates over Φ_{HS} .

In order to check the quality of this result, we compare the compressibility factor $Z=\beta p/\rho$, where the pressure is $p=-\partial F/\partial V$ and the total density ρ in this case $\rho=\rho_A$, against simulation results for $q=10$ in Fig. 4(a). Also shown are results for the pure hard sphere case. The compressibility factor is considerably larger for amphiphiles than for spheres. This is to be expected, as we compare states with equal packing fractions of spheres, but with (amphiphiles) and without (spheres) tails. The interactions of the tails with the sphere lead to the observed increase by more than a factor of 2. The shapes of both curves, however, are similar. The theoretical results are slightly smaller than the MC data, but the general agreement is remarkable. Finally, we note that Z is a quite sensitive quantity. Recall that our approximation is on the level of F^{exc} , and Z is obtained by differentiation and division by density, operations which in general will enhance any deviations. We also plot the low-density behavior governed by the second virial coefficient both from DFT and from the exact calculation. They essentially coincide on the resolution of the plot.

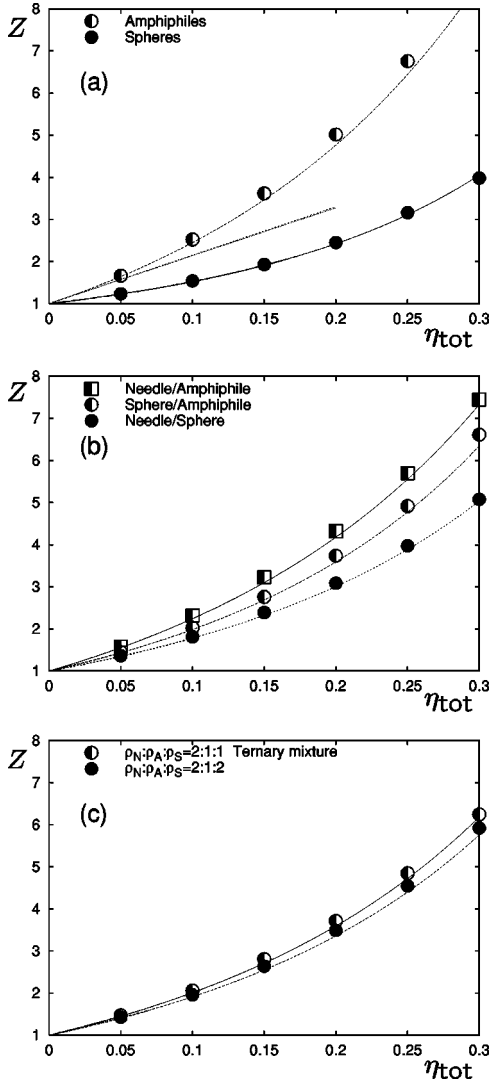


FIG. 4. Compressibility factor Z as a function of total packing fraction η_{tot} . Simulation results (symbols) are compared against theoretical predictions (lines). Straight lines indicate the low-density limit governed by the second virial coefficient. (a) Pure systems; (b) binary mixtures; (c) ternary mixtures.

B. Binary mixtures

Once a system possess two distinguishable components, it may undergo a demixing phase transition into two macroscopically distinct phases with different compositions of particles. In our case, binary mixtures are obtained by setting the density of one of the species of the ternary mixture to zero. For these systems, we shall investigate how the size ratio q plays the role of a control parameter for demixing behavior, and especially enlighten the limits $q \rightarrow 0, \infty$. Then we focus on the interesting question of how amphiphiles mix with either needles or spheres, compared to the mixing behavior of needles and spheres.

1. Needles and spheres

According to computer simulation results by Bolhuis and Frenkel [31], a mixture of spheres and infinitely thin needles displays a demixing phase transition into a sphere-rich

(needle-poor) phase and a sphere-poor (needle-rich) phase. The mechanism for this phase separation is, crudely speaking, the gain in configurational entropy in both demixed phases. In the needle-rich phase, interactions are considerably reduced, because the needles do not interact among themselves, and the presence of spheres is only a perturbing ‘‘impurity’’ effect to essentially an ideal gas of needles. The sphere-rich phase, however, is only weakly disturbed by the presence of the needles [32]. Bolhuis and Frenkel developed a first order perturbation theory that is similar to Lekkerkerker’s free volume approach for the Asakura-Oosawa colloid-ideal-polymer mixture. The present DFT approach recovers their result [32]; the excess free energy per volume is

$$\frac{\beta F^{\text{exc}}}{V} = \Phi_{\text{HS}}(\eta_S) + \rho_N \left[\frac{3q\eta_S}{4(1-\eta_S)} - \ln(1-\eta_S) \right]. \quad (19)$$

It is interesting to compare this result with that of the above case of pure amphiphiles, Eq. (18). To do so, we naively set $\rho_S = \rho_N$, and compare with Φ_A for a single component. The results are not identical (which should not be expected), but differ by a logarithmic expression. Its origin can be traced back to the fact that the needles in the binary mixture are individual particles with an Euler characteristic of unity. In the case of amphiphiles, the needle tails alone have vanishing Euler characteristic, and the corresponding term in the free energy functional vanishes (in bulk). Note also that this term is independent of q (as is the Euler characteristic). In summary, we stress that Φ_A cannot be obtained by the trivial restriction of equal densities in the free energy of the binary sphere-needle mixture. The naive calculation yields an additional term in the compressibility, which is q independent and given by $\eta_A/(1-\eta_A)$. This is a small contribution for large q , but destroys the hard sphere limit for $q \rightarrow 0$, which is correct in the proper DFT result.

As was already found in Ref. [31], a comparison with the simulation results demonstrates the excellent quality of the equation of state obtained from the theory. We repeat this comparison in Fig. 4(b), using the compressibility factor from both simulation and theory. Indeed, both results are in good agreement.

In the case of the needle-sphere binary mixture the analytic expression for the spinodal was found to be [32]

$$\rho_N \pi q^2 R^3 = \frac{4(1+2\eta_S)^2}{3\eta_S}. \quad (20)$$

This is universal (q independent) in the ‘‘natural’’ variables η_S and $\rho_N q^2 R^3$. Note that $\rho_N q^2$ is exactly the proper scaling in the Onsager limit. The critical point in the limit $q \rightarrow \infty$ is $q \rho_N R^3 = \pi [1 + (44/3)q^{-1} + O(q^{-2})]$ and $q \eta_S = (4/3) [1 - (28/3)q^{-1} + O(q^{-2})]$. We display the demixing phase diagram in Fig. 5 for $q = 10, 20, 50$, as well as the metastable (with respect to freezing) [31] case $q = 0$. For small densities the system is in a mixed state; increasing density leads to demixing. The critical point moves toward smaller η_S as q grows.

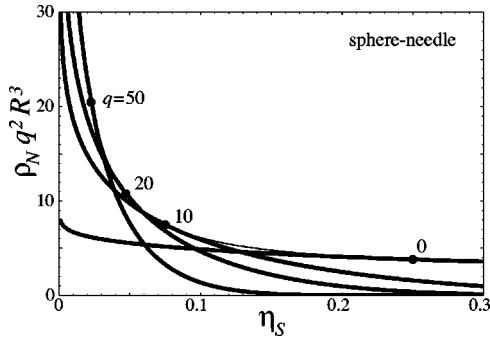


FIG. 5. Phase diagram for the sphere-needle mixture for $q = 10, 20, 50$ as a function of sphere packing fraction η_S and scaled needle density $\rho_N q^2 R^3$. The binodals (thick lines), q -independent spinodal (thin line), and critical points (dots) are shown.

2. Amphiphiles and needles

Adding needles to a fluid phase of amphiphiles should be easier than adding needles to a hard sphere fluid of the same density: The amphiphile tails are expected to create free volume for the needles, an effect that is absent in the case of hard spheres as a host fluid. The excess free energy for the amphiphile-needle mixture is

$$\frac{\beta F^{\text{exc}}}{V} = \Phi_A(\eta_A) + \rho_N \left[\frac{3q\eta_A}{4(1-\eta_A)} - \ln(1-\eta_A) \right]. \quad (21)$$

This result is the same as in the case of the sphere-needle mixture, but with Φ_{HS} replaced by Φ_A . Hence the contribution due to the presence of the free needles is the same in both cases. In other words, the free needles interact only with the heads of the amphiphiles. Clearly, this is true for the interaction potentials. On the level of the free energy, it represents an approximation and will not hold in general for the exact free energy. See Fig. 4(b) for comparison with the simulation results.

The demixing spinodal of the amphiphile-needle binary mixture is

$$\rho_N \pi L^2 R = \frac{4(1+2\eta_A)^2}{3\eta_A} + 2q(1-\eta_A). \quad (22)$$

We next investigate the limit of short needles, $q \rightarrow 0$. At fixed scaled density $\rho_N \pi L^2 R$, the model reduces to the sphere-needle mixture. This is physically reasonable, because the amphiphile shape reduces essentially to a sphere to which only a very short needle is attached. The latter should not matter. The free needles still play a role, because their density ρ_N grows large as $\rho_N \pi L^2 R$ is kept constant. See Fig. 6 for the demixing phase diagram as a function of η_A and $q^2 \rho_N$ for $q=0, 10, 20$. As q increases, the spinodals shift to higher densities, and the critical point moves to smaller η_A . In the case of long rods, $q \rightarrow \infty$, the location of the critical point is $q \rho_N R^3 = (4/\pi)[1 + 2q^{-1} + O(q^{-2})]$ and $q \eta_A = (2/3)[1 - 2q^{-1} + O(q^{-2})]$.

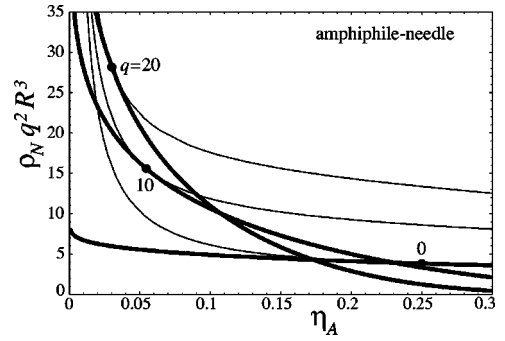


FIG. 6. Phase diagram for amphiphile-needle mixture for $q = 0, 10, 20$. The dots mark the critical points. The case $q=0$ is equal to the sphere-needle binary mixture.

3. Amphiphiles and spheres

The excess free energy is

$$\frac{\beta F^{\text{exc}}}{V} = \Phi_{\text{HS}}(\eta_{\text{tot}}) + \frac{9q\eta_A\eta_{\text{tot}}}{16\pi R^3(1-\eta_{\text{tot}})}, \quad (23)$$

where $\eta_{\text{tot}} = \eta_S + \eta_A$. Here both densities are intimately coupled, through Φ_{HS} as a function of the total packing fraction. The additional contribution is again linear in q , and has a similar but not identical dependency on the densities as in the other cases. See Fig. 4(b) for comparison with the simulation results:

The spinodal for the amphiphile-sphere binary mixture is obtained as

$$\begin{aligned} \rho_A 8\pi(q'-1)R^3/3 \\ = 1 + q' - \eta_S(q'-1)(q'+2) \\ + \sqrt{3q'(1+q'/3)[1 + \eta_S(q'-1)(q'\eta_S-2)]}, \end{aligned} \quad (24)$$

where $q' = 3q/8$.

We next discuss the limiting cases. Clearly, for needles with vanishing length $q=0$, the amphiphiles reduce to spheres, and the system reduces to pure hard spheres. A particularly interesting case is the crossover between short and long needle tails. For amphiphiles with large q , the system demixes. For small q the phase transition is clearly absent, as both species become identical. The interesting question is how the crossover between the two cases happens. We find that demixing is absent for $q < q^* = 8/3$. If q^* is approached from above, the spinodal shifts to large amphiphile densities, and diverges formally. However, this scenario is likely to be preempted by freezing. For long needles $q \rightarrow \infty$, the effect of the attached head groups vanishes, and the amphiphiles behave like effective needles. Hence the model reduces to the needle-sphere mixture. As regards the spinodal, the limit is attained at quite large size ratios q .

In Fig. 7(a) we display the demixing phase diagram as a function of both packing fractions η_S and η_A . In order to have packing fractions inside the assumed fluid region, we use the rough criterion $\eta_S + \eta_A < 0.5$, which is about the value at freezing of pure hard spheres. Rather long needle tails with $q > 20$ are needed to access this region. The limit

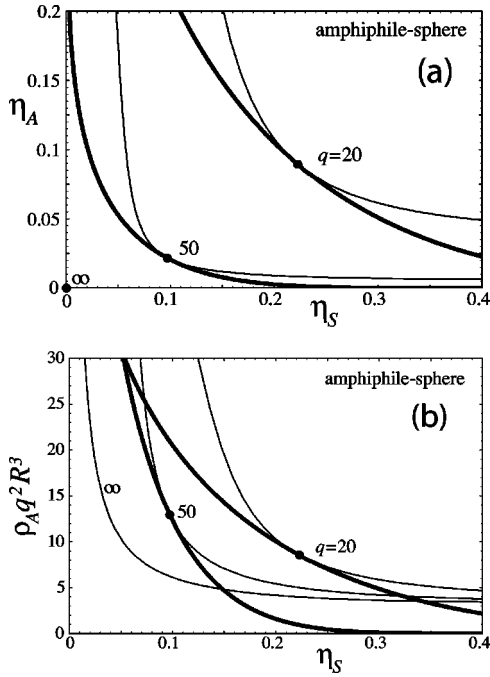


FIG. 7. Phase diagram for the amphiphile-sphere mixture for $q=20,50,\infty$: (a) as a function of η_S and η_A ; (b) as a function of η_S and $\rho_A q^2$. The case $q=\infty$ is equal to the (universal) result for the sphere-needle binary mixture.

$q \rightarrow \infty$ can be traced by using the scaled density $\rho_A q^2 R^3$ instead of the packing fraction; see Fig. 7(b). In this representation, a well-defined limiting curve is obtained, which again coincides with the universal needle-sphere spinodal.

Let us discuss the disappearance of the demixing transition in both binary systems that contain amphiphiles. This crucially depends on the size ratio q . In the case of the amphiphile-needle mixture, increasing q leads to a suppression of demixing, i.e., to a shift toward higher densities. In contrast, for amphiphile-sphere mixtures, *decreasing* q is necessary to suppress demixing. In conclusion, q tunes the character of the amphiphiles, whether spherophile (small q) or needle loving (large q).

4. Comparison of binary mixtures

The sphere-needle mixture will constitute our reference system, with which we compare both other binary subsystems possessing amphiphiles. The amphiphile-needle system can be regarded as a derivative of the needle-sphere system that is obtained by replacing each sphere particle in the needle-sphere system with an amphiphile particle. It is interesting to investigate the differences of these two similar systems, namely, to monitor the effect of the attached needles. In Fig. 8(a) we show the demixing phase behavior as a function of packing fraction and scaled needle density. In order to compare with the needle-sphere mixture, we use η_A and η_S as variables for the respective systems. Hence we compare states with the same packing fraction of spheres, whether these are part of amphiphiles (in the amphiphile-needle case) or free (in the sphere-needle case). We observe that the amphiphile-needle system demixes for considerably

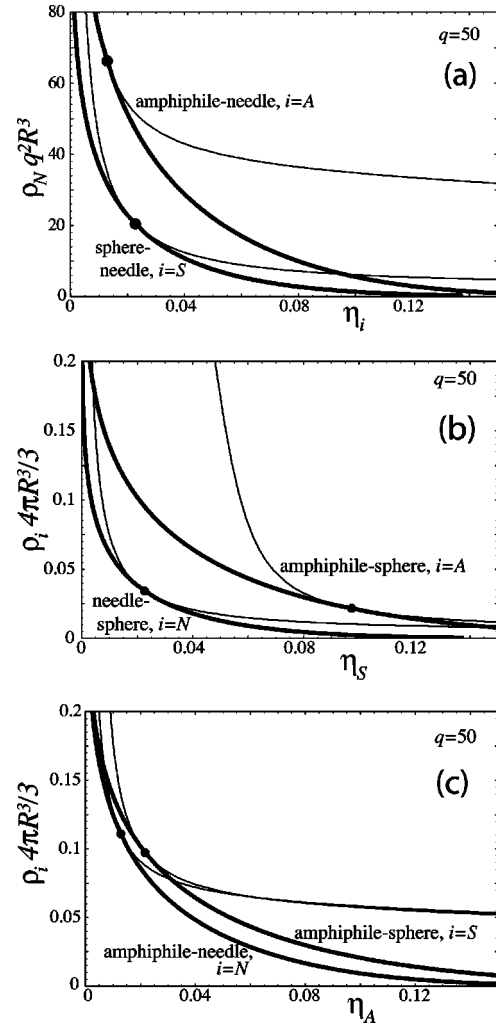


FIG. 8. Comparison of phase diagrams for different binary mixtures at $q=50$. Thick lines are binodals, thin lines spinodals, and the dots mark the critical points. (a) Sphere-needle and amphiphile-needle; (b) sphere-needle and amphiphile-sphere; (c) amphiphile-needle and amphiphile-sphere.

higher densities than the sphere-needle system, i.e., it still remains in a mixed state after the sphere-needle system has already undergone the demixing transition. Note that this happens even though the amount of particle ‘‘material’’ is larger in the amphiphile-needle case due to the additional presence of the amphiphile tails. However, this is precisely what is expected for amphiphilic behavior: The amphiphiles mix better with the needle phase than do pure spheres.

Next we seek to investigate how the behavior of the amphiphile-sphere system changes, if we replace the amphiphiles with needles. In Fig. 8(b) we compare both phase diagrams for $q=50$ as a function of sphere packing fraction η_S and the respective densities ρ_A and ρ_N , which we scale with the volume of a sphere $4\pi R^3/3$. The amphiphile-needle demixing curve is shifted toward larger densities compared to the sphere-needle case. This means that amphiphiles mix better with spheres than pure needles do. Again, this behavior is precisely the expected one for particles with amphiphilic character.

The final comparison aims at the question of which species, needles or spheres, mixes better with amphiphiles. In Fig. 8(c) the amphiphile-needle phase diagram is compared with the amphiphile-sphere phase diagram. As variables, we use the packing fraction of spheres and the number densities of either spheres or needles (again scaled by the volume of a sphere). The amphiphile-sphere spinodal is at slightly higher densities. The difference decreases upon increasing q . So the tendencies of spheres and needles to mix with amphiphiles are roughly equal (and become identical for $q \rightarrow \infty$).

In summary, we observe a strong shift of the coexistence lines toward higher densities in those systems where particles are replaced by amphiphiles. Note that all our comparisons are done at equal densities. This also means that in the case with amphiphiles space is more density filled with particles, because amphiphiles are larger than either spheres or needles. In spite of this, the system favors the mixed state. All these findings strongly support the initial assumption, that our model particles indeed possess amphiphilic character.

C. Ternary mixture

For the three-component system of spheres, needles, and amphiphiles, the Helmholtz excess free energy per volume for homogeneous, isotropic states is

$$\frac{\beta F^{\text{exc}}}{V} = \Phi_{\text{HS}}(\eta_{\text{tot}}) + \rho_N \left[\frac{3q\eta_{\text{tot}}}{4(1-\eta_{\text{tot}})} - \ln(1-\eta_{\text{tot}}) \right] + \frac{9q\eta_A\eta_{\text{tot}}}{16\pi R^3(1-\eta_{\text{tot}})} \quad (25)$$

$$= -[\rho_N + 3\eta_{\text{tot}}/(4\pi R^3)] \ln(1-\eta_{\text{tot}}) + \frac{3\eta_{\text{tot}}}{16\pi R^3(1-\eta_{\text{tot}})^2} [6\eta_{\text{tot}}(2-\eta_{\text{tot}}) + 3q(1-\eta_{\text{tot}})] \times (\eta_{\text{tot}} - \eta_S) + 4\pi q R^3 \rho_N (1-\eta_{\text{tot}}). \quad (26)$$

From the excess pressure $p_{\text{exc}} = -\partial F^{\text{exc}}/\partial V = -\Phi + \sum_i \rho_i \partial \Phi / \partial \rho_i$, we obtain the (excess) compressibility factor as

$$\frac{\beta p_{\text{exc}}}{\rho} = \frac{\eta_{\text{tot}}}{4(1-\eta_{\text{tot}})^3} \left\{ (1-\eta_{\text{tot}})[3q+4(1-\eta_{\text{tot}})] + 9 \frac{4\eta_{\text{tot}} - q\eta_S(1-\eta_{\text{tot}})}{3\eta_{\text{tot}} + 4\pi R^3 \rho_N} \right\}, \quad (27)$$

where $\rho = \rho_A + \rho_N + \rho_S$ is the total density. We compare this expression with results from computer simulations in Fig. 4(c) for two different compositions of species, and find good agreement over the entire density range considered.

The density ρ_N^r in a reservoir of needles that is in equilibrium with the system is related to the system density via $\rho_N = \rho_N^r \exp(-\beta\mu_N)$, where the (reduced) excess chemical potential for the needles is $\beta\mu_N = \partial \Phi / \partial \rho_N$. Here the result is

$$\rho_N = \rho_N^r (1 - \eta_{\text{tot}}) \exp\left(-\frac{3q\eta_{\text{tot}}}{4(1-\eta_{\text{tot}})}\right), \quad (28)$$

which has the same structure as in the sphere-needle binary case, except that the *total* number of spheres contributes through η_{tot} , not only the free ones through η_S . It is the total packing fraction of spheres, whether pure or the heads of amphiphiles, that interacts with the needles.

A complete investigation of the demixing phase diagram of the ternary mixture is beyond the scope of the present work, and we restrict ourselves to a study of the spinodal. The spinodal for the full three-component system can be obtained as

$$\rho_N \pi R^3 q^2 = \frac{1}{\eta_{\text{tot}}} \left[\frac{4}{3} (2\eta_{\text{tot}} + 1)^2 + 2q\eta_A(1-\eta_{\text{tot}}) - \frac{3}{4} q^2 \eta_A (\eta_{\text{tot}} - \eta_A) \right], \quad (29)$$

where $\eta_{\text{tot}} = \eta_A + \eta_S$. This is an explicit expression for the needle density ρ_N as a function of the densities of spheres and amphiphiles. It can easily be converted into reservoir representation using Eq. (28). Given the complexity of the model containing three species, two of them possessing anisotropic shapes, we find it quite remarkable that a simple expression can be obtained for an (approximate) spinodal. Note that for fixed size ratio q the ternary mixture has three thermodynamic variables, namely, the densities of the three species. The spinodal is a two-dimensional manifold, which is embedded in the three-dimensional phase space.

VI. CONCLUSIONS AND OUTLOOK

We have proposed a hard body model for a ternary amphiphilic mixture. Water molecules are represented by hard spheres, oil molecules by infinitely thin hard needles, and amphiphiles are a hybrid of both. Clearly, this can at best mimic the complex molecular interactions in a real system. Nevertheless, our model features *continuous* degrees of freedom, in contrast to widely used lattice models. Our aim was to demonstrate that this model carries various characteristics of real amphiphilic mixtures. Using a specifically designed density functional theory, we have investigated the bulk fluid demixing phase diagram, and have discussed its rich behavior, demonstrating that phase boundaries are qualitatively in accordance with physical expectation. We expect that our theory accounts also for inhomogeneities on small length scales similar to the particle dimensions. As its hard sphere counterpart (Rosenfeld's functional) yields excellent results when compared to simulations, we expect a similar quality of results for our system. Such applications to inhomogeneous situations have been left out of the current work. The next step is to show whether the model exhibits lamellar and micellar phases. Their existence is crucial to the ability of the hard body amphiphile mixture to describe real systems.

As possible further directions of research, we mention the question of how freezing of hard spheres is affected by the presence of amphiphiles, as well as the nature of the solid phases built by the amphiphiles, which poses a challenging

packing problem. Furthermore, the study of the interfaces between demixed phases will be especially intriguing due to the number and nature of the different phases in the bulk phase diagram. This touches on the very relevant question of how the amphiphiles are arranged at the oil-water interface.

Concerning the general status of the theory, we are faced with an important example where geometry-based DFT yields previously unknown bulk thermodynamics. This is in contrast to the cases of hard spheres, the Asakury-Oosawa model, and Bolhuis-Frenkel's needle-sphere mixture, where expressions from scaled-particle or free volume theory were previously known, and where these results were rederived by

DFT. Geometry-based DFT is a systematic way to treat such hard core systems, whereas the scaled-particle or free volume approaches require considerable physical insight to be formulated. This is an advantage in terms of comprehensibility; however, it becomes increasingly difficult to apply these approaches to more complex systems like the one considered in this work.

ACKNOWLEDGMENT

One of us (M.S.) would like to thank B. Mulder for an inspiring discussion.

-
- [1] S. H. Chen, J. S. Huang, and P. Tartaglia, *Structure and Dynamics of Strongly Interacting Colloids and Supramolecular Aggregates in Solution* (Kluwer Academic Publishers, Dordrecht, 1992).
- [2] W. M. Gelbart, D. Roux, and A. Ben-Shaul, in *Micelles, Membranes, Microemulsions and Monolayers*, edited by S. H. Chen, J. S. Huang, and P. Tartaglia (Springer, Berlin, 1994).
- [3] J. Meunier, D. Langevin, and N. Boccarda, *Physics of Amphiphilic Layers* (Springer, Berlin, 1987).
- [4] R. Lipowsky, D. Richter, and K. Kremer, *The Structure and Conformation of Amphiphilic Membranes* (Springer, Berlin, 1992).
- [5] B. Widom, *J. Chem. Phys.* **84**, 6943 (1986).
- [6] A. Ciach and J. S. Hoye, *J. Chem. Phys.* **95**, 5300 (1991).
- [7] K. A. Dawson, M. P. Lipkin, and B. Widom, *J. Chem. Phys.* **88**, 5149 (1988).
- [8] G. Gompper and M. Schick, in *Micelles, Membranes, Microemulsions and Monolayers* (Ref. [2]).
- [9] G. Gompper and M. Schick, *Self-Assembling Amphiphilic Systems* (Academic Press, London, 1994).
- [10] C. N. Likos, K. R. Mecke, and H. Wagner, *J. Chem. Phys.* **102**, 9350 (1995).
- [11] R. Evans, in *Fundamentals of Inhomogeneous Fluids*, edited by D. Henderson (Dekker, New York, 1992), p. 85.
- [12] A. M. Somoza, E. Chacón, L. Mederos, and P. Tarazona, *J. Phys.: Condens. Matter* **7**, 5753 (1995).
- [13] S. de Miguel and M. M. T. da Gama, *J. Chem. Phys.* **107**, 6366 (1997).
- [14] C. Guerra, A. M. Somoza, and M. M. T. da Gama, *J. Chem. Phys.* **109**, 1152 (1998).
- [15] C. Guerra, A. M. Somoza, and M. M. T. da Gama, *J. Chem. Phys.* **111**, 7646 (1999).
- [16] D. Duque and P. Tarazona, *J. Chem. Phys.* **107**, 10 207 (1997).
- [17] P. Tarazona, D. Duque, and E. Chacon, *Phys. Rev. E* **62**, 7147 (2000).
- [18] I. Napari, A. Laaksonen, and R. Strey, *J. Chem. Phys.* **113**, 4476 (2000).
- [19] I. Napari, A. Laaksonen, and R. Strey, *J. Chem. Phys.* **113**, 4480 (2000).
- [20] V. Talanquer and D. W. Oxtoby, *J. Chem. Phys.* **113**, 7013 (2000).
- [21] H. Löwen, in *Spatial Statistics and Statistical Physics*, edited by K. R. Mecke and D. Stoyan, *Lecture Notes in Physics*, Vol. 554 (Springer, Berlin, 2000).
- [22] Y. Rosenfeld, *Phys. Rev. Lett.* **63**, 980 (1989).
- [23] Y. Rosenfeld, M. Schmidt, H. Löwen, and P. Tarazona, *J. Phys.: Condens. Matter* **8**, L577 (1996).
- [24] Y. Rosenfeld, M. Schmidt, H. Löwen, and P. Tarazona, *Phys. Rev. E* **55**, 4245 (1997).
- [25] P. Tarazona, *Phys. Rev. Lett.* **84**, 694 (2000).
- [26] Y. Rosenfeld, *Phys. Rev. E* **50**, R3318 (1994).
- [27] J. A. Cuesta, *Phys. Rev. Lett.* **76**, 3742 (1996).
- [28] J. A. Cuesta and Y. Martinez-Raton, *Phys. Rev. Lett.* **78**, 3681 (1997).
- [29] M. Schmidt, H. Löwen, J. M. Brader, and R. Evans, *Phys. Rev. Lett.* **85**, 1934 (2000).
- [30] M. Schmidt, *Phys. Rev. E* **63**, 010101(R) (2001).
- [31] P. Bolhuis and D. Frenkel, *J. Chem. Phys.* **101**, 9869 (1994).
- [32] M. Schmidt, *Phys. Rev. E* **63**, 050201(R) (2001).
- [33] M. Elbaum, D. K. Fyngenson, and A. Libchaber, *Phys. Rev. Lett.* **76**, 4078 (1996).
- [34] D. K. Fyngenson, M. Elbaum, B. Shraiman, and A. Libchaber, *Phys. Rev. E* **55**, 850 (1997).
- [35] K. Lin, J. C. Crocker, A. C. Zeri, and A. G. Yodh, *Phys. Rev. Lett.* **87**, 088301 (2001).